On the conceptual equivalence of embedded strong discontinuity and smeared crack formulations

G. N. Wells* L. J. Sluys

Koiter Institute Delft
Delft University of Technology
P.O. Box 5048, 2600 GA Delft, The Netherlands

Abstract

Embedded discontinuity formulations have been recently presented as a method of incorporating displacement discontinuities in standard finite elements. These elements allow inelastic deformations to be modelled using discrete constitutive models at an internal interface. However, the actual formulation of these models is identical in concept to more traditional fracture energy regularised smeared crack models. Rather than adjusting the hardening modulus depending on element size, the inelastic strain itself is made dependent on element size. It is shown here that the embedded discontinuity idea and smeared crack models are conceptually identical.

Keywords
Embedded discontinuity, smeared cracks, concrete fracture.

1 Introduction

Smeared crack models are commonly used for the failure analysis of materials such as concrete. Cracking is simulated by introducing strain softening into the classical continuum formulation [1–6]. Despite the theoretical flaws of these models, they are simple and with careful use can provide remarkably good predictions of actual responses. Importantly, the deficiencies and limitations of theses models are well recognised. The key issue is that the finite element size must be included directly in the constitutive model to make the energy dissipated in failure objective.

A more recent development in the analysis of localised failure are 'embedded discontinuity' elements. These elements attempt to include the effect of a discontinuity in the displacement field as an incompatible strain mode [7–11]. In some forms, these models allow the direct application of discrete (traction–separation) constitutive models [9, 11]. In this case, no length scales from the finite element mesh appear directly in the constitutive model (unlike smeared models), rather a length scale is included in the element formulation itself through the form of the incompatible strain modes. Unlike smeared formulations where the hardening modulus is adapted depending on the element size, the inelastic strain itself is adapted according the to element size. This makes identification of the element length scales involved more difficult.

*Corresponding author e-mail: g.wells@citg.tudelft.nl, Fax: +31 15 278 6383

To elucidate the similarities between embedded discontinuity and smeared crack formulations, the embedded discontinuity formulation is first presented. It is then shown how the embedded discontinuity model can be formulated at integration point level. The formulation at integration point level is compared with traditional smeared crack models and the similarities are highlighted. The intention of this paper is to emphasise the equivalence of strong embedded discontinuities and the smeared crack idea and dispel the notation that embedded discontinuities models can capture displacement discontinuities.

2 Strong embedded discontinuity formulation

The most successful of the strong embedded discontinuity approaches is that based on the work of Simo et al. [7] for one-dimensional problems, which has been extended to two dimensions by Oliver [8] and Armero and Garikipati [9] and to three dimensions byWells and Sluys [11]. This formulation is developed from both kinematic and kinetic considerations, and has been termed the 'statically and kinematically optimal model' [12]. A detailed discussion and comparison of the different formulations can be found in [12]. These formulations should be restricted to constant strain elements, the reason for which are discussed in Wells [13].

The standard embedded discontinuity formulation is based on the *enhanced assumed strain* (EAS) concept [14]. The object of this work is to show the conceptual equivalence of the embedded discontinuity model and smeared crack models, so the governing equations for the embedded discontinuity model are simply presented and not derived. The weak governing equations for the strong embedded discontinuity model are expressed as [8, 9, 11]:

$$\int_{\Omega} \mathbf{B}^{\mathrm{T}} \boldsymbol{\sigma} \, \mathrm{d}\Omega - \int_{\Gamma_u} \mathbf{N}^{\mathrm{T}} \bar{\mathbf{t}} \, \mathrm{d}\Gamma = \mathbf{0} \tag{1a}$$

$$\int_{\Omega_e} \mathbf{G}^{*\mathrm{T}} \boldsymbol{\sigma} \, \mathrm{d}\Omega + \int_{\Gamma_{d_e}} \mathbf{t} \, \mathrm{d}\Gamma = \mathbf{0} \quad \forall \, \Omega_e. \tag{1b}$$

where $\mathbf{N}$ and $\mathbf{B}$ are matrices containing the usual displacement and strain interpolations (from the compatible part of the displacement field), respectively, $\boldsymbol{\sigma}$ is a vector containing components of the stress tensor, $\mathbf{t}$ are the traction forces acting at a discontinuity, $\bar{\mathbf{t}}$ are tractions acting on an external boundary and $\mathbf{G}^*$ is a matrix containing interpolations of the variations of the enhanced strain. Equation (1a) is the standard virtual work equation, and equation (1b) governs the enhanced strains. The enhanced strains are incompatible, and therefore equation (1b) is applied for each element crossed by a discontinuity. Equation (1b) applies for all elements crossed by a discontinuity. The matrix $\mathbf{G}^*$ has the form:

$$\mathbf{G}_e^* = \frac{A_e}{V_e} \mathbf{n}_e \tag{2}$$

where A_e is the area of the discontinuity plane through an element, V_e is the volume of

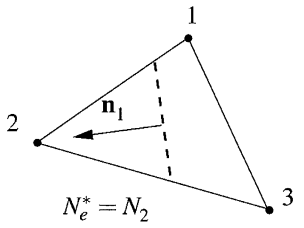

Figure 1: Node associated with N_e^*.

the element and the matrix $\mathbf{n}_e$ is of the form:

$$\mathbf{n}_e = \begin{bmatrix} n_1 & 0 & 0 \\ 0 & n_2 & 0 \\ 0 & 0 & n_3 \\ n_2 & n_1 & 0 \\ 0 & n_3 & n_2 \\ n_3 & 0 & n_1 \end{bmatrix} \tag{3}$$

where n_1, n_2 and n_3 are the components of the unit vector $\mathbf{n}$ for an element. The strain at a point in an element is calculated using:

$$\boldsymbol{\varepsilon} = \mathbf{B}\mathbf{a} + \mathbf{G}\boldsymbol{\alpha} \tag{4}$$

where $\mathbf{a}$ are the regular nodal displacements and $\boldsymbol{\alpha}$ are the enhanced nodal displacements at a discontinuity (representing the displacement jump components). The displacement jump components are internal degrees of freedom of an element. The matrix $\mathbf{G}_e$ for an element has the form:

$$\mathbf{G}_e = - \begin{bmatrix} \frac{\partial N_e^*}{\partial x_1} & 0 & 0 \\ 0 & \frac{\partial N_e^*}{\partial x_2} & 0 \\ 0 & 0 & \frac{\partial N_e^*}{\partial x_3} \\ \frac{\partial N_e^*}{\partial x_2} & \frac{\partial N_e^*}{\partial x_1} & 0 \\ 0 & \frac{\partial N_e^*}{\partial x_3} & \frac{\partial N_e^*}{\partial x_2} \\ \frac{\partial N_e^*}{\partial x_3} & 0 & \frac{\partial N_e^*}{\partial x_1} \end{bmatrix} \tag{5}$$

where N_e^* is the shape function associated with the node which is 'alone' on one side of the discontinuity. This is illustrated in figure 1 for a three-noded element. The test functions for the enhanced strain ($\mathbf{G}^*$) are not the same as the trial functions ($\mathbf{G}$). The test functions are formulated to impose traction continuity within elements. The trial functions are formed based on kinematic considerations. It will be shown in the following section that if $\mathbf{G}^*$ is used for both the test and trial function, the formulation is *identical* to classical smeared formulations. A detailed discussion of the need for kinematic enhancements can be found in [12].

The stress rate in terms of nodal displacement velocities is given by:

$$\dot{\boldsymbol{\sigma}} = \mathbf{D}\left(\mathbf{B}\dot{\mathbf{a}} + \mathbf{G}\dot{\boldsymbol{\alpha}}\right) \tag{6}$$

where $\mathbf{D}$ is a material tangent matrix relating the stress and strain rates. The traction rate at a discontinuity is given by:

$$\dot{\mathbf{t}} = \mathbf{T}\dot{\boldsymbol{\alpha}} \tag{7}$$

where $\mathbf{T}$ is the tangent relating the traction rate and the displacement jump rate. To form the element stiffness matrix, the stress and traction rate expressions are inserted into the weak governing equations in (1). This yields for an element:

$$\begin{bmatrix} \mathbf{K}_{bb,e} & \mathbf{K}_{bg,e} \\ \mathbf{K}_{g^*b,e} & \mathbf{K}_{g^*g,e} + \mathbf{K}_{t,e} \end{bmatrix} \begin{Bmatrix} d\mathbf{a}_e \\ d\boldsymbol{\alpha}_e \end{Bmatrix} = \begin{Bmatrix} \mathbf{f}^{\text{ext}}_{u,e} \\ \mathbf{0} \end{Bmatrix} - \begin{Bmatrix} \mathbf{f}^{\text{int}}_{u,e} \\ \mathbf{f}^{\text{int}}_{\alpha,e} \end{Bmatrix} \tag{8}$$

where

$$\mathbf{K}_{bb,e} = \int_{\Omega_e} \mathbf{B}_e^{\mathrm{T}} \mathbf{D} \mathbf{B}_e \, d\Omega \tag{9a}$$

$$\mathbf{K}_{bg,e} = \int_{\Omega_e} \mathbf{B}_e^{\mathrm{T}} \mathbf{D} \mathbf{G}_e \, d\Omega \tag{9b}$$

$$\mathbf{K}_{g^*b,e} = \int_{\Omega_e} \mathbf{G}_e^{*\mathrm{T}} \mathbf{D} \mathbf{B}_e \, d\Omega \tag{9c}$$

$$\mathbf{K}_{g^*g,e} = \int_{\Omega_e} \mathbf{G}_e^{*\mathrm{T}} \mathbf{D} \mathbf{G}_e \, d\Omega \tag{9d}$$

$$\mathbf{K}_{t,e} = \int_{\Gamma_{d},e} \mathbf{T}_e \, d\Gamma \tag{9e}$$

$$\mathbf{f}^{\text{ext}}_{u,e} = \int_{\Gamma_{u},e} \mathbf{N}_e^{\mathrm{T}} \bar{\mathbf{t}} \, d\Gamma \tag{9f}$$

$$\mathbf{f}^{\text{int}}_{u,e} = \int_{\Omega_e} \mathbf{B}_e^{\mathrm{T}} \boldsymbol{\sigma} \, d\Omega \tag{9g}$$

$$\mathbf{f}^{\text{int}}_{\alpha,e} = \int_{\Omega_e} \mathbf{G}^{*\mathrm{T}}_e \boldsymbol{\sigma} \, d\Omega + \int_{\Gamma_{d},e} \mathbf{t}_e \, d\Gamma \tag{9h}$$

and $d\mathbf{a}_e$ and $d\boldsymbol{\alpha}_e$ are the iterative-incremental displacements. The subscript 'e' has been added to denote that the stiffness matrix is for a single element. Note that irrespective of the material model used, the element stiffness matrix is non-symmetric. This is a result of the Petrov-Galerkin type formulation ($\mathbf{G} \neq \mathbf{G}^*$).

3 Integration point level formulation

Usually, the incompatible strain modes in the model presented in the previous section are solved using standard static condensation procedures. In this way, the internal degrees of freedom do not enter the global system of equations. From equation (8), the condensed stiffness matrix and internal force vector can be expressed as:

$$\mathbf{K}_{\text{con},e} = \mathbf{K}_{bb,e} - \mathbf{K}_{bg,e} \left[\mathbf{K}_{g^*g,e} + \mathbf{K}_{t,e} \right]^{-1} \mathbf{K}_{g^*b,e} \tag{10}$$

$$\mathbf{f}^{\text{int}}_{\text{con},e} = \mathbf{f}^{\text{int}}_{u,e} - \mathbf{K}_{bg,e} \left[\mathbf{K}_{g^*g,e} + \mathbf{K}_{t,e} \right]^{-1} \mathbf{f}^{\text{int}}_{\alpha,e} \tag{11}$$

The condensed element stiffness matrices and internal force vectors are used in assembly of the global system of equations. After solving the global system of equations for the iterative-incremental displacements $d\mathbf{a}$ via

$$d\mathbf{a} = [\mathbf{K}_{\text{con}}]^{-1} \left\{ \mathbf{f}_u^{\text{ext}} - \mathbf{f}_{\text{con}}^{\text{int}} \right\}, \tag{12}$$

the iterative-incremental displacements at the discontinuity within an element can be found.

$$d\boldsymbol{\alpha}_e = -\left[\mathbf{K}_{g^* g,e} + \mathbf{K}_{t,e} \right]^{-1} \left[\mathbf{K}_{g^* b,e} d\mathbf{a}_e + \mathbf{f}_{\alpha,i}^{\text{int}} \right] \tag{13}$$

Assuming an elastic response in the continuum, from equation (10), the condensed element stiffness matrix is expressed as:

$$\begin{aligned} \mathbf{K}_{\text{con},e} = & \int_{\Omega_e} \mathbf{B}^{\text{T}} \mathbf{D}^{\text{e}} \mathbf{B} \, d\Omega \\ & - \int_{\Omega_e} \mathbf{B}^{\text{T}} \mathbf{D}^{\text{e}} \mathbf{G} \, d\Omega \left(\int_{\Omega_e} \mathbf{G}^{*\text{T}} \mathbf{D}^{\text{e}} \mathbf{G} + \int_{\Gamma_{d,e}} \mathbf{T}_e \, d\Gamma \right)^{-1} \int_{\Omega_e} \mathbf{G}^{*\text{T}} \mathbf{D}^{\text{e}} \mathbf{B} \, d\Omega \end{aligned} \tag{14}$$

where $\mathbf{D}^{\text{e}}$ is the elastic material tangent. For constant strain elements, the integrals in equation (14) can be eliminated,

$$\mathbf{K}_{\text{con,e}} = V_e \mathbf{B}^{\text{T}} \mathbf{D}^{\text{e}} \mathbf{B} - V_e \mathbf{B}^{\text{T}} \mathbf{D}^{\text{e}} \mathbf{G} \left(V_e \mathbf{G}^{*\text{T}} \mathbf{D}^{\text{e}} \mathbf{G} + A_e \mathbf{T}_e \right)^{-1} V_e \mathbf{G}^{*\text{T}} \mathbf{D}^{\text{e}} \mathbf{B}. \tag{15}$$

Defining a matrix $\tilde{\mathbf{D}}$ as:

$$\tilde{\mathbf{D}} = V_e \mathbf{D}^{\text{e}} \mathbf{G} \left(V_e \mathbf{G}^{*\text{T}} \mathbf{D}^{\text{e}} \mathbf{G} + A_e \mathbf{T}_e \right)^{-1} \mathbf{G}^{*\text{T}} \mathbf{D}^{\text{e}} \tag{16}$$

and then considering the definition of the matrix $\mathbf{G}^*$ in equation (2),

$$\tilde{\mathbf{D}} = \mathbf{D}^{\text{e}} (-\mathbf{G}) \left(\mathbf{n}_e^{\text{T}} \mathbf{D}^{\text{e}} (-\mathbf{G}) + \mathbf{T}_e \right)^{-1} \mathbf{n}_e^{\text{T}} \mathbf{D}^{\text{e}}. \tag{17}$$

Note that $\mathbf{n}_e$ is not the normal vector to a discontinuity, rather it is a matrix that contains components of the normal vector (see equation (3)). Using the result in equation (17), equation (15) can be rearranged to yield:

$$\mathbf{K}_{\text{con},e} = V_e \mathbf{B}^{\text{T}} \underbrace{\left(\mathbf{D}^{\text{e}} - \tilde{\mathbf{D}} \right)}_{\mathbf{D}} \mathbf{B} \tag{18}$$

where $\mathbf{D}$ is the equivalent continuum tangent, showing that the EAS-based model can be cast in an equivalent continuum format and solved using a conventional Bubnov-Galerkin procedure. This applies for both the symmetric ($\mathbf{G} = \mathbf{G}^*$) and non-symmetric (Petrov-Galerkin) models. The tangent $\mathbf{D}$ in equation (18) is almost identical in form to the more traditional smeared crack formulation [2, 4]. The only difference to the smeared crack formulation for a single crack is the matrix $\mathbf{G}$, which is a measure of the element size and reflects the element geometry. For the symmetric approach ($\mathbf{G} = \mathbf{G}^*$), the matrix $\tilde{\mathbf{D}}$ is equal to:

$$\tilde{\mathbf{D}} = \mathbf{D}^{\text{e}} \mathbf{n}_e \left(\mathbf{n}_e^{\text{T}} \mathbf{D}^{\text{e}} \mathbf{n}_e + \frac{V_e}{A_e} \mathbf{T}_e \right)^{-1} \mathbf{n}_e^{\text{T}} \mathbf{D}^{\text{e}} \tag{19}$$

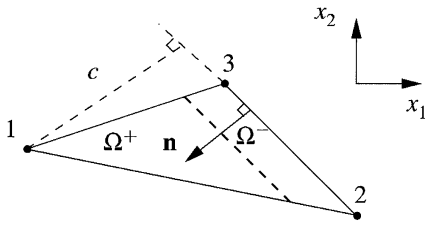

Figure 2: Triangular element crossed by a discontinuity (represented by the dashed line) with the discontinuity aligned with an element edge.

which is symmetric. The only difference with smeared crack formulations is the inclusion of the scalar V_e/A_e in the tangent, which is a measure of element size. This avoids the need to adjust the hardening modulus element-wise, since the element length scale is already included in the formulation. In light of this equivalence of the embedded discontinuity formulation and classical smeared crack models, it must be concluded that many of the difficulties which dog classical smeared crack models will persist.

Since the embedded discontinuity model can be cast in a conventional finite element setting, with a non-linear continuum constitutive operator, it shows that the model is actually *continuous*.

4 Implications of the non-symmetric formulation

In this section, the implications of the kinematically formulated trial functions are examined. For the element shown in figure 2, N_e^* is equal to the shape function N_1 of node one and the discontinuity through the element is aligned with one edge of the element. Through some simple calculations it can be shown that:

$$\nabla N_e^* = \begin{Bmatrix} \dfrac{\partial N_1}{\partial x_1} \\ \dfrac{\partial N_1}{\partial x_2} \end{Bmatrix} = \frac{1}{c} \begin{Bmatrix} n_1 \\ n_2 \end{Bmatrix} \tag{20}$$

where c is a scalar (shown in figure 2) and n_1 and n_2 are components of the normal vector in the x_1 and x_2 directions, respectively. Comparing the matrices in equations (5) and (3), the qualitative difference between the matrices $\mathbf{G}^*$ and $\mathbf{G}$ disappears, with $\mathbf{G}$ being a scalar multiple of $\mathbf{G}^*$. Therefore, for the case when a discontinuity is aligned with an element edge, $\mathbf{G} = (V_e c/A_e)\mathbf{G}^*$. This result is not surprising when considering that conventional smeared models perform well when an element edge is aligned in the direction of the crack or shear band. From figure 2 and equation (20), the kinematic enhancement can be considered as projecting a discontinuity such that it is parallel to an element side, a case in which conventional finite elements are known to perform well. The scalar c provides a measure of the element size and the 'normal vector' is not dependent on the discontinuity orientation, rather the spatial orientation of the element edge. The motivation for the enhanced strain field given by Oliver [8] that the 'incompatible displacement' equals $\mathscr{H}_{\Gamma_d} - N_e^*$ which is chosen since it is equal to zero at element nodes thus seems improper and gives an incorrect justification to the

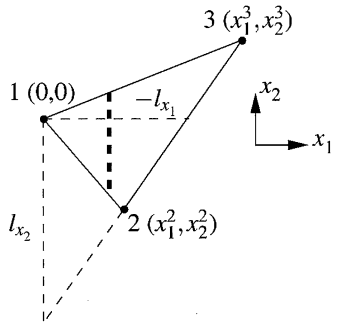

Figure 3: Element length scales implied by the kinematic enhancement.

kinematic enhanced strain field. The kinematic enhancement simply makes the strain enhancement element-dependent. The enhancement is dependent not only on element size, but also element orientation.

It must be emphasised that the use of the function N_e^* introduces numerical length scales to the formulation. Taking the gradient of N_e^* can be considered as a sophisticated measure of the width of an element. From equation (20), the gradient ∇N_e^* implies a length scale and an element-dependent normal vector. Alternatively (and equivalently), it can be considered to imply two element length scales. Consider the element shown in figure 3. The element is crossed by a discontinuity such that N_e^* is equal to the shape function of node one, N_1. Through algebraic manipulations, it can be shown that $\partial N_e^*/\partial x_1 = 1/l_{x_1}$ and $\partial N_e^*/\partial x_2 = 1/l_{x_2}$, where l_{x_1} and l_{x_2} are shown graphically in figure 3. Defining the 'enhanced kinematic strains' $\tilde{\boldsymbol{\varepsilon}}^k$ as

$$\tilde{\boldsymbol{\varepsilon}}^k = \mathbf{G}\boldsymbol{\alpha}, \tag{21}$$

(cf. equation (4)) the kinematic enhanced continuum strains in terms of a displacement jump are expressed as:

$$\tilde{\varepsilon}_{11}^k = -\frac{\alpha_{x_1}}{l_{x_1}} \tag{22a}$$

$$\tilde{\varepsilon}_{22}^k = -\frac{\alpha_{x_2}}{l_{x_2}} \tag{22b}$$

$$2\tilde{\varepsilon}_{12}^k = -\frac{\alpha_{x_1}}{l_{x_2}} - \frac{\alpha_{x_2}}{l_{x_1}}. \tag{22c}$$

Equation (22) shows that use of the kinematic enhancement implies a different numerical length scale in each spatial direction in the global coordinate system. This can be compared to the symmetric enhancement where only one length scale, $l = A_e/V_e$, is implied. The kinematic enhancement is intimately related to element size and shape.

5 Single-edge notched (SEN) beam

A single-edge notched beam, as test experimentally by Schlangen [15], is analysed using the embedded discontinuity model. Figure 4 shows the embedded cracks for a

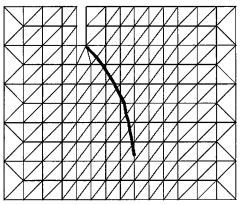

Figure 4: Two-dimensional SEN beam with crack path continuity enforced.

two-dimensional analysis. Through the enforcement of crack path continuity (in a geometric sense), a curved crack path can be calculated [16]. However, the calculations could not performed further than the point in figure 4 due to the inability of the elements to 'transfer' the effect of the crack to elements ahead of the crack tip [13]. Using the embedded element technique leads to similar convergence problems as observed with a smeared crack approach.

6 Conclusions

It has been shown that so-called 'embedded discontinuity' models are conceptually equivalent to classical smeared crack models and will therefore inherit the undesirable properties of classical smeared models. Since the Heaviside jump does not appear explicitly in the formation, and the displacement jump is incompatible, the embedded discontinuity model is *not* discontinuous. This adds to the appeal of more recent methods in which the Heaviside jump does appear explicitly in the formulation and the displacement jump is compatible [17].

Acknowledgements

This research is supported by the Technology Foundation STW, applied science division of NWO and the technology program of the Ministry of Economic Affairs and the Ministry of Public Works and Water Management, The Netherlands.

References

[1] Bažant ZP, Oh B. Crack band theory for fracture of concrete. *RILEM Mat. Struct.* 1983; **16**(93):155–177.

[2] De Borst R, Nauta P. Non-orthogonal cracks in a smeared finite element model. *Engng. Comp.* 1985; **2**(1):35–46.

[3] Willam K, Pramono E, Sture S. Fundamental issues of smeared crack models. In *SEM-RILEM International Conference on Fracture of Concrete and Rock*, SP Shah, SE Swartz, eds. Springer-Verlag, Houston, Texas 1987; 142–157.

[4] Rots JG. *Computational modeling of concrete fracture.* Ph.D. thesis, Delft University of Technology 1988.

[5] Oliver J. A consistent characteristic length for smeared cracking models. *Int. J. Numer. Meth. Engng.* 1989; **28**(2):461–474.

[6] Feenstra PH, De Borst R. A plasticity model and algorithm for mode-I cracking in concrete. *Int. J. Numer. Meth. Engng.* 1995; **38**(15):2509–2529.

[7] Simo JC, Oliver J, Armero F. An analysis of strong discontinuities induced by strain-softening in rate-independent inelastic solids. *Comp. Mech.* 1993; **12**:277–296.

[8] Oliver J. Modelling strong discontinuities in solid mechanics via strain softening constitutive equations. Part 2: Numerical simulation. *Int. J. Numer. Meth. Engng.* 1996; **39**(21):3601–3623.

[9] Armero F, Garikipati K. An analysis of strong discontinuities in multiplicative finite strain plasticity and their relation with the numerical simulation of strain localization. *Int. J. Solids & Structures* 1996; **33**(20–22):2863–2885.

[10] Larsson R, Runesson K. Element-embedded localization band based on regularized displacement discontinuity. *ASCE J. Eng. Mech.* 1996; **122**(5):402–411.

[11] Wells GN, Sluys LJ. Three–dimensional embedded discontinuity model for brittle fracture. *Int. J. Solids & Structures* 2001; **38**(5):897–913.

[12] Jirásek M. Comparative study on finite elements with embedded discontinuities. *Comput. Methods Appl. Mech. Engrg.* 2000; **188**(1–3):307–330.

[13] Wells GN. *Discontinuous modelling of strain localisation and failure.* Ph.D. thesis, Delft University of Technology 2001.

[14] Simo JC, Rifai MS. A class of mixed assumed strain methods and the method of incompatible modes. *Int. J. Numer. Meth. Engng.* 1990; **29**(8):1595–1638.

[15] Schlangen E. *Experimental and numerical analysis of fracture processes in concrete.* Ph.D. thesis, Delft University of Technology 1993.

[16] Alfaiate J, Wells GN, Sluys LJ. On the use of embedded discontinuity elements with crack path continuity for mode-I and mixed-mode fracture. *Engng. Fracture Mech.* 2002; **69**(6):661–686.

[17] Wells GN, Sluys LJ. A new method for modelling cohesive cracks using finite elements. *Int. J. Numer. Meth. Engng.* 2001; **50**(12):2667–2682.